Munera, S.; Aleixos Borrás, MN.; Besada, C.; Gómez-Sanchis, J.; Salvador, A.; Cubero, S.; Talens Oliag, P.... (2019). Discrimination of astringent and deastringed hard "Rojo Brillante" persimmon fruit using a sensory threshold by means of hyperspectral imaging. Journal of Food Engineering. 263:173-180. https://doi.org/10.1016/j.jfoodeng.2019.06.008

Discrimination of astringent and deastringed hard 'Rojo Brillante' persimmon fruit using a sensory threshold by means of hyperspectral imaging

Sandra Munera[a], Nuria Aleixos[b], Cristina Besada[c], Juan Gómez-Sanchís[d] Alejandra Salvador[e], Sergio Cubero[f], Pau Talens[g], José Blasco[h]*

[a)] Centro de Agroingeniería. Instituto Valenciano de Investigaciones Agrarias (IVIA). Ctra. Moncada-Náquera Km 4.5, 46113, Moncada, Valencia (Spain). *Corresponding author: blasco_josiva@gva.es Tel.: +34 961465315

[b)] Departamento de Ingeniería Gráfica. Universitat Politècnica de València. Camino de Vera, s/n, 11 46022 Valencia (Spain).

[c)] Centro de Poscosecha. Instituto Valenciano de Investigaciones Agrarias (IVIA). Ctra. Moncada-Náquera Km 4.5, 46113, Moncada, Valencia (Spain).

[d)] Departamento de Ingeniería Electrónica. Universitat de València. Av. Universitat, s/n, 46100 Burjassot, Valencia (Spain).

[e)] Departamento de Tecnología de Alimentos. Universitat Politècnica de València. Camino de Vera, s/n, 46022 Valencia (Spain).

Abstract

Persimmon fruit cv. 'Rojo Brillante' is an astringent cultivar due to its content of soluble tannins, which are insolubilised during the ripening of the fruit. Traditionally, the consumption of this cultivar has only been possible when the fruit is overripe and the texture is soft. Postharvest treatments based on exposing fruits to high CO_2 concentrations allow astringency removal while preserving high flesh firmness. However, the effectiveness of this treatment is controlled by means of slow destructive methods. The aim of this work is to study the application of hyperspectral imaging in the spectral range 450-1040 nm to discriminate astringent (A) and deastringed (DA) fruits non-destructively. To separate both type of fruit, it was used a threshold of soluble tannins based on sensorial perception (0.04 % of fresh weight). The spectral information from three different areas of each fruit (calyx, middle and apex) was

used to build models to predict the soluble tannins (ST) content using partial least squares regression (PLS-R). The results using this method indicated that it was not possible to accurately discriminate fruit with levels of ST below 0.04 %, especially in the case of DA fruits (42.2%). Thus, another classification models were performed using partial least squares discriminant analysis (PLS-DA) that included other properties in order to discriminate between A and DA using the ST threshold. The most accurate models using all and optimal wavelengths selected were those which focused on the middle and apex areas of the fruit, a correct classification rate of 87.0% being achieved for A fruits and above 84.4% for DA fruits. To date, there are only subjective and destructive analytical methods to monitor the effectiveness of the astringency removal treatments in persimmon. The results obtained in this study indicate that hyperspectral images can therefore be considered as an objective and non-destructive alternative in the control of this process.

Keywords*: Diospyros kaki; astringency; soluble tannins; computer vision; chemometrics*

Abbreviations

A = astringent

CV = cross validation

CI = colour index

DA = deastringed

F = firmness

LV = latent variable

PLS-R = partial least squares regression

PLS-DA = partial least squares discriminant analysis

RMSE = root mean squared error

R^2 = coefficient of determination

RPD = ratio of performance to deviation

ST = soluble tannins

58 TSS = total soluble solids

1. INTRODUCTION

Spain is the number one producer of persimmon fruit *(Diospyros kaki)* in Europe and the third largest producer in the world, after China and South Korea (FAOSTAT, 2016). In the last twenty years, the land area devoted to cultivating this crop has risen from 2,000 to 14,000 ha, and production has increased from 33 to 310 thousand tons (FAOSTAT, 2016). Part of this growth is due to the increase in the production of the 'Rojo Brillante' cultivar in the Mediterranean area. This cultivar, like other persimmon cultivars, is astringent at harvest and must be subjected to post-harvest treatments to remove astringency. The development of the de-astringency methods based on high CO_2 concentrations allowed removal of the astringency while preserving high flesh F (Arnal and Del Río, 2003), which has facilitated a rapid commercial expansion of this crop. Nowadays 'Rojo Brillante' persimmon is one of the most appreciated persimmon cultivars worldwide.

The conditions considered as standard for the complete elimination of astringency in this cultivar are 95% CO_2 for 18-24 h at 20ºC. Under these conditions, the ST, responsible for astringency, are polymerised by the acetaldehyde produced to form insoluble compounds, which are non-astringent (Matsuo and Itoo, 1982; Taira et al., 1997; Salvador et al., 2008). However, the treatment may not be completely effective when the conditions of the process are not well controlled (Arnal & Del Río, 2003). In addition, the effectiveness of the treatment is also severely affected by the physiological state of the fruit. Small changes in the cellular structure can make the diffusion of CO_2 through the spaces difficult, the result being a low rate of anaerobic respiration and consequently less accumulation of acetaldehyde. This, in turn, leads to a lesser reduction of the ST (Salvador et al., 2007).

To commercialise this fruit, it is necessary to guarantee the complete removal of the astringency, since the presence of any astringency in the fruit can cause rejection by the consumer that will in turn affect future sales. The control of residual astringency in the fruits after the treatments can be performed destructively by measuring ST in the fruit using the Folin–Denis method (Arnal and Del Río, 2004). However, in addition to being destructive, this method is slow and requires specialised equipment and personnel. An alternative is based on the

reaction of the ST with $FeCl_3$. Tannic acid complexes with ferric iron may consist of large highly coloured molecules that behave as colloids. Mixing them gives rise to a ferric complex that causes an intense black colour. The intensity of the black stain observed after impregnating a slice of the flesh with $FeCl_3$ reveals the presence of ST in the fruit and its intensity depends on their level (Gorini and Testoni, 1988; Munera et al., 2017). Although this method is faster and easier than the analytical determination of ST, it is still destructive and subjective. Therefore, it is necessary to search for new rapid, reliable and non-destructive techniques.

An alternative is based on the use of optical methods. Hyperspectral imaging is a promising optical technique for quality inspection of agricultural and food products that incorporates the main advantages of spectroscopy and imaging (Lorente et al., 2012). Thus, hyperspectral imaging can simultaneously acquire spectral and spatial information. In addition, the equipment used can be sensitive to different regions of the electromagnetic spectrum, such as the ultraviolet or infrared regions (Gomez-Sanchís et al., 2014; Cortés et al., 2018). Their use has been widely studied to control the quality of fruit and vegetables during postharvest, for example to discriminate similar cultivars of nectarines with different properties (Munera et al., 2018), to discriminate gluten-free oats from cereals with gluten (Erkinbaev, Henderson and Paliwal, 2017), to detect decay lesions in citrus fruits (Folch-Fortuny et al., 2016) or mechanical damage in potatoes (López-Maestresalas et al., 2016). In recent years, several studies have been conducted to predict the content of ST or to assess the astringency in different varieties of persimmon fruit using spectroscopy (Zhang et al., 2013; Noypitak et al., 2015; Altieri et al., 2017; Cortés et al., 2017) and hyperspectral imaging (Munera et al., 2017). These works included the study of the best area of the fruit to measure the astringency, since the internal distribution may vary from the calyx area to the bottom. Most of the studies report successful prediction or classification models but they are not useful for precise prediction in fruits with low ST content, since they achieved limits of detection much higher than the minimum content of ST (0.10 %) that causes a sensation of astringency for most cultivars (Vidrih et al., 1994; Antoniolli et al., 2000; Antoniolli et al., 2003).

In the case of 'Rojo Brillante', ST values above 0.06% can produce sensory astringency (Besada et al., 2010). Throughout the season, fruits of this cultivar exhibit high astringency at harvest time with an ST content of between 0.80% and 0.40% (Salvador et al., 2007). Only when the fruit is over-ripe (which causes the total loss of F) does the loss of sensorial astringency occur. In that moment, the ST is around 0.04% (Tessmer et al., 2016). In other studies in which the de-astringency treatment with high CO_2 concentration has been applied, an effective treatment has been associated with ST values of 0.01-0.03% (Salvador et al., 2007; Salvador et al., 2008; Besada et al., 2008).

Hence, the main objective of this work was to study the application of hyperspectral imaging to predict the ST content in persimmon fruits and to discriminate astringent (A) from deastringed (DA) persimmons using 0.04 % of ST as the threshold. Moreover, in order to establish a practical tool for use in industry, another goal is to determine which part of the fruit is the most appropriate to measure, as well as to reduce the amount of spectral information generated and speed up this process.

2. MATERIAL AND METHODS

2.1 Fruit samples and experimental design

In this study, 300 persimmon fruits cv. 'Rojo Brillante' with similar size and no signs of external defects were analysed. In order to obtain fruit with different degrees of ripeness, 100 fruits were harvested every week over three consecutive weeks. The fruits were collected from an orchard in L'Alcúdia (Valencia, Spain) at commercial maturity. The maturity index used for harvesting was the external colour index (CI) of the fruit. The CI commonly employed for 'Rojo Brillante' is $CI = (1000a)/(Lb)$, where L, a and b are the colour coordinates in HunterLab colour space (Salvador et al., 2007). The average CI of the fruit at each harvest was 2.5, 3.9 and 9.3, respectively.

In each harvest, three homogeneous lots of fruit were submitted to different treatments to obtain fruit with different levels of ST, as follows: i) de-astringency treatment for 24 hours (40 fruits); ii) de-astringency treatment for 12 hours (30 fruits); and iii) no de-astringency treatment

142 (30 fruits). In all cases, the de-astringency treatment was applied under standard conditions
143 (95% CO_2, at 20ºC, 90% RH). Hyperspectral images and the reference analyses were performed
144 within 8 h after the treatment.
145
146 **2.2 Hyperspectral imaging acquisition**
147 The hyperspectral imaging system consisted of an industrial camera (CoolSNAP ES,
148 Photometrics, AZ, USA) coupled to two liquid-crystal tuneable filters (Varispec VIS-07 and
149 NIR-07, Cambridge Research & Instrumentation, Inc., MA, USA). The camera was configured
150 to acquire images with a size of 1392 × 1040 pixels and a spatial resolution of 0.14 mm/pixel.
151 The working spectral range was defined between 450 nm and 1040 nm, capturing images every
152 10 nm. Thus, hypercubes with 60 images were captured. In order to avoid problems of
153 unfocused images due to the refraction of light across this wide spectral range, the focus was
154 adjusted on the central band of the acquisition interval (740 nm) and the images were captured
155 using lenses capable of covering the whole spectral range without going out of focus (Xenoplan
156 1.4/23, Schneider Optics, Hauppauge, NY, USA). To optimise the dynamic range of the camera,
157 prevent the images from saturated regions and correct the spectral sensitivity of the different
158 elements of the system, the maximum integration time of each band was calibrated by capturing
159 the averaged grey level of a white reference standard (Spectralon 99%, Labsphere, Inc, NH,
160 USA), corresponding to 90 % of the dynamic range of the camera.
161 The scene was illuminated using diffuse light from twelve halogen spotlights (37 W)
162 (Eurostar IR Halogen MR16. Ushio America, Inc., CA, USA) powered by direct current (12 V)
163 and arranged equidistant from each other inside a hemispherical aluminium diffuser. The inner
164 surface of the aluminium diffuser was painted white with a rough texture to maximise its
165 reflectivity and minimise directional reflections, which could cause bright spots, the result being
166 highly homogeneous light.
167 The fruits were introduced manually into a fruit holder in three different positions so as to
168 obtain images from the top part of the fruit, the side, and the bottom. In this study, we have
169 referred these areas as calyx, middle and apex areas respectively (Figure 1). Thus, three

hyperspectral images were acquired for each fruit using customised software developed at IVIA, a total of 900 images being obtained.

2.3 Reference analysis

The skin colour of each fruit was measured using a colorimeter (CR-300, Konica Minolta Inc., Tokyo, Japan). The mean value of the *L*, *a* and *b* colour coordinates (HunterLab colour space) was obtained as the average of three measurements in different parts of the fruit. The total colour difference (ΔE) between A and DA fruits was calculated by Equation (1):

$$\Delta E = \sqrt{(L_A - L_{DA})^2 + (a_A - a_{DA})^2 + (b_A - b_{DA})^2} \quad (1)$$

The F of the flesh was determined by means of a universal testing machine (4301, Instron Engineering Corp., MA, USA) equipped with an 8-mm puncture probe. The crosshead speed during testing was 1 mm/s. During the test, the force increased smoothly until it decreased drastically when the flesh was broken, and then the maximum peak force was registered. The results were expressed as the load (in N) required to break the flesh of the fruit on both sides after peel removal.

In order to assess the astringency of the fruits, each fruit was divided into two halves: one half was pressed against a 10 × 10 cm filter paper soaked in a 5% $FeCl_3$ solution, which produced a dark print whose distribution and intensity gave information about the ST content in the flesh (Figure 2). The other half was used to obtain the ST content by the Folin-Denis method (Taira, 1995) based on the reduction of the Folin-Ciocalteu reagent by ST in alkaline solution (Arnal and Del Río, 2004). Taking into account the heterogeneous distribution of the tannins in the flesh (Figure 2), the samples for destructive analysis were taken from the lower part and near the apex, since the tannins take longer to be removed in this part.

The ANOVA, followed by Tukey's honestly significant difference test, was conducted using the software Statgraphics (Manugistics Corp., Rockville, USA) to find significant differences in the results of the physicochemical analysis related to the length of the de-astringency treatment.

The groups of samples met the following three requirements: i) the observations being tested are independent within and among the groups; ii) the groups associated with each mean in the test are normally distributed; and iii) there is equal within-group variance across the groups associated to each mean in the test (homogeneity of variance).

2.4 Image pre-processing

The reflectance captured by the camera is influenced by the intensity of the incoming light, the sensitivity of the sensor of the camera and the sensitivity of the LCFT, at the different wavelengths (Geladi, 2007). Thus, there is a need to correct these effects to obtain the true reflectance of the sample. This is done using a reflectance standard (Spectralon 99%, Labsphere, Inc, NH, USA) through Equation (2) (Gat, 2000):

$$\rho_{xy}(x,y,\lambda) = \frac{\mathrm{R^{abs}}}{\mathrm{R^{abs}_{white}}} = \rho^{\mathrm{Ref}}(\lambda)\frac{\mathrm{R(x,y,\lambda)-R_{black}(x,y,\lambda)}}{\mathrm{R_{white}(x,y,\lambda)-R_{black}(x,y,\lambda)}} \quad (2)$$

where ρ_{xy} is the reflectance of the fruit, $\rho^{Ref}(\lambda)$ is the standard reflectance of the white reference target (99 % in this work), $R(x,y,\lambda)$ is the radiance of the fruit captured by the CCD sensor of the camera, $R_{white}(x,y,\lambda)$ is the radiance captured by the CCD of the white reference target, and $R_{black}(x,y,\lambda)$ is the radiance captured by the CCD while avoiding any light source in order to quantify the electronic noise of the CCD.

The average reflectance spectrum of each area of each fruit was determined by averaging the relative reflectance spectra of all pixels included in the fruit area. This process was performed using a binary mask. To do so, a threshold was established between the background and the fruit at the wavelength of the greatest contrast between the two regions (700 nm). This provided an easy way to remove the background of the image from the fruit. In the case of the calyx view, this also allowed the leaves to be removed from the analyses. As the contrast was so high, the segmentation was quite accurate.

These operations were performed using HYPER-Tools (Mobaraki and Amigo, 2018) working under MATLAB R2017b (The MathWorks, Inc., MA, USA).

2.5 Multivariate data analysis

After the analysis of the ST content and knowing which fruit was A and DA, the spectra were randomly partitioned into two sets. For each area of the persimmon fruit, 201 fruit spectra (107 A and 94 DA) were used to calibrate the models and 99 fruit spectra (54 A and 45 DA) were used for independent validation or test set.

PLS-R was used to quantify the ST content and PLS-DA was used to classify the fruits as A and DA according to the threshold value of 0.04% (Tesmeer et al., 2016). A model using the spectral information of each area (calyx, middle and apex) was performed.

Previously, the mean spectrum of each area of the persimmon fruit was filtered using the Savitzky-Golay second derivative (3-point smoothing window, second-order polynomial) to remove both additive and multiplicative effects, and pre-treated using standard normal variate to remove the scatter (Rinnan et al., 2009). Later, each resulting spectrum was normalised by mean centre. A 10-fold CV was used to obtain the optimal number of LVs as well as an estimation of the error rate of the models. The PLS-R models were evaluated by the R^2 and the RMSE between the predicted and the measured value of the reference parameter for calibration, CV and prediction. Furthermore, the RPD, defined as the ratio between the standard deviation of the reference data and $RMSE_P$, was used (Williams, 1987). The results of the PLS-DA models were expressed as the percentage of correct classification (percentage of A or DA fruits correctly classified) and total accuracy (percentage of all fruits correctly classified) for calibration, CV and prediction.

In order to reduce the dimensionality of the hyperspectral images, the vector of regression coefficients was used. This method measures the association between each wavelength and the response (i.e. A and DA class) obtained by the PLS-DA model (Mehmood et al., 2012). The wavelengths with a high absolute value are selected, since they make the highest contribution to the classification, and those with a smaller absolute value are ignored.

252 The spectral pre-processing was carried out using HYPER-Tools (Mobaraki and Amigo,
253 2018) and the PLS models were performed using MATLAB R2017b (The MathWorks, Inc.,
254 MA, USA).
255
256 **3. RESULTS AND DISCUSSION**
257 **3.1 Reference analysis**
258 In general, the ST content in the fruits ranged from 1.18 % (non-treated fruits) to 0.01 %
259 (fruit treated for 24 hours), while those fruits that were non-treated presented ST values from
260 0.37 % to 1.18 %, depending on the time of harvesting (Table 1).
261
262 Table 1. Soluble tannins content and quantification of astringent and deastringed fruits

Harvest	Treatment duration	Soluble tannins (%)			#A	#DA
		Min	Mean	Max		
1	0h	0.37	0.69[b]	0.98	48	52
	12h	0.02	0.09[e]	0.33		
	24h	0.01	0.02[f]	0.03		
2	0h	0.45	0.61[c]	0.77	53	47
	12h	0.01	0.11[e]	0.31		
	24h	0.02	0.03[f]	0.04		
3	0h	0.66	0.91[a]	1.18	60	40
	12h	0.10	0.37[d]	0.66		
	24h	0.02	0.03[f]	0.04		
Total		0.01	0.32	1.18	161	139

263 *Different letters indicate significant differences between groups (p-value<0.05), according to*
264 *Tukey's (HSD) test. Min = minimum; Max = maximum; #A = number of astringent fruits;*
265 *#DA = number of deastringed fruits*
266
267 Thus, the mean value of the fruits collected in different moments was statistically different.
268 The CO_2 treatment for 12 hours resulted in fruits with a wide range of ST values between 0.66
269 % and 0.01 %. This meant that part of the fruits could already be consumed while others still
270 needed more hours of treatment. In this case, the mean values of the three harvests were also
271 statistically different. When the treatment was applied for 24 hours, all fruits reached an eatable

stage and no statistical differences were found among the three times of harvesting. Using the threshold of 0.04% for the ST value, a total of 161 fruits were considered as A and 139 as DA (Table 1).

The application of a de-astringency treatment with CO_2 does not usually have any effect on the colour in the early stages of ripeness. Only slight differences could be observed between A and DA fruit coordinates (Table 2). Although significant differences were found between *L* and *b*, they are barely perceptible to the human eye. According to the International Commission on Illumination (CIE), the value of ΔE obtained (1.9) indicates that, in general, the colour difference between the two classes of fruits is minimally perceptible (Mokrzycki and Tatol, 2011).

Table 2. Skin colour of astringent and deastringed fruits

	L (*)			*a*			*b (*)*			ΔE	CI		
	Min	Mean	Max	Min	Mean	Max	Min	Mean	Max		Min	Mean	Max
A	56.0	62.8	67.9	1.9	11.7	25.6	32.6	37.1	41.0	1.9	-0.03	5.1	13.5
DA	56.8	62.2	67.5	-2.25	13.4	30.5	32.3	36.7	41.7		-1.08	5.9	14.7

(*) indicate significant differences between groups (p-value<0.05). Min = minimum; Max = maximum; A = astringent; DA = deastringed; CI = colour index

As in the case of the colour, CO_2 treatment does not usually affect the F of the fruit in the early stages of ripeness. However, it does give rise to a significant degree of softening in the following stages. These changes in firmness are related to the changes that take place in the cell structure (Salvador et al., 2007). Here, the mean value of the F was reduced from 47.3 N in A fruits to 43.7 N in DA fruits (Table 3).

Table 3. Flesh firmness of astringent and deastringed fruits

	Flesh firmness (N) (*)		
	Min	Mean	Max
A	37.4	47.3	58.9
DA	29.9	43.7	54.5

(*) indicate significant differences between groups (p-value<0.05). Min = minimum; Max = maximum; A = astringent; DA = deastringed

3.2 Spectral analysis

The average spectra obtained for each measured area of A and DA fruits are illustrated in Figure 3. The spectra of all fruits followed a similar pattern in each area. Slight differences were present in the VIS region around 460 nm, 550-600 nm and 650-710 nm, where carotenoids, anthocyanins, chlorophylls and other pigments are responsible for fruit colour (Rajkumar et al., 2012). In the NIR region, some differences were found, especially in the apex area, around 750 nm, where a water absorption peak (OH second overtone) is observed (Siedliska et al., 2018; Williams and Norris, 1987). Noypitak et al. (2015) indicated that phenolic compounds are located between 940-1000 nm and the absorption peak of tannic acid is seen at 996 nm. In this case, slight differences were found close to these wavelengths between the A and DA spectra. However, it is not clear whether this corresponded to the ST content because a water absorption peak (third overtone of OH stretching vibration) dominates this part of the spectrum (Nicolaï et al., 2007).

3.3 Prediction of soluble tannins content

PLS-R models were performed to quantify the content of ST in each fruit using the spectral range of 450-1050 nm. Table 4 shows the results of the prediction of ST content obtained for the three areas of the fruit that were measured.

The optimal model was chosen when the number of LV yields the lowest RMSE for calibration and CV. Therefore, 15 LVs were determined for the calibration of the model of the calyx area, 12 for the middle area model and 13 for the apex area model. The model using the spectra obtained from the calyx area achieved the lowest R^2 (0.49) while the highest RMSE (0.25 %) was obtained in the test set. In contrast, the model built for the middle area offered better results, with an R^2 of 0.69 and an RMSE of 0.19 %, while the model obtained for the apex area achieved the highest R^2 and the lowest RMSE of 0.73 and 0.18 %, respectively. The RPD

values indicate that only the models that used measurements obtained in the middle and apex areas could discriminate between low and high ST values (RPD values between 1.5 and 2) (Nicolai et al., 2007). However, in all cases, the RMSE value was higher than the 0.04 % threshold, which means that the models were not altogether useful for accurate prediction in fruits with extremely low ST content.

Table 4. Results of calibration and validation of the models to predict the ST content using hyperspectral imaging and the different areas of the fruit

Area	#LV	Calibration		Cross validation		Prediction		
		R^2	RMSE	R^2	RMSE	R^2	RMSE	RPD
Calyx	15	0.71	0.18	0.54	0.23	0.49	0.25	1.4
Middle	12	0.71	0.17	0.60	0.21	0.69	0.19	1.8
Apex	13	0.76	0.16	0.64	0.20	0.73	0.18	1.9

#LV = number of latent variables

The scientific literature contains other studies that achieve findings similar to ours but using mostly spectroscopy instead of hyperspectral imaging. For example, Noypitak et al. (2015) used interactance mode in the evaluation of ST using different areas of persimmons cv. 'Xichu', achieving, as best result, an R^2 of 0.93 and a high RMSE of 0.22 % but using the calyx area. However, the higher R^2 was probably achieved because most of the persimmons used had very low (0.02 %) or very high (1.6 %) tannin contents and only a few samples had intermediate values. In the case of 'Rojo Brillante', Cortés et al. (2017) developed models using spectra pre-treated with different techniques, achieving better results in terms of R^2 (0.91) and RMSE, above 0.08 %, using six measurement points distributed throughout the fruit.. In this case, the ST content ranged from 0.023 to 0.75 but DA fruit were 20 %, while in our case they represent 46 % of the fruit in the models. Moreover, most of the error is introduced by fruits with very low ST values. Alitieri et al. (2017) also achieved a good prediction result with an R^2 higher than 0.98 but in the cross validation set and using fruits with ST content values between 0.1 %

and 1.7 %, which should be considered as astringent in all cases from a commercial point of view.

Figure 4 shows the prediction performance of the model using the test set and the data captured in the apex area. Taking into account the threshold of 0.04 %, only 77.8 % of A fruits and 42.2 % of DA fruits were correctly predicted. These results are clearly low and below those expected. Thus, the direct prediction of very low values of ST content (such as 0.04 %) does not seem to be possible with the procedure followed. This is probably because the concentration of ST is correlated with other major biochemical constituents such as pigments, water or other soluble solids like sugars that can mask the detection of constituents when the content is very low (Nicolaï et al., 2007). For this reason, a different approach to measuring astringency other than the direct estimation of ST was required. PLS-DA models were then developed to maximise the separation between classes A and DA, not only with respect to the differences in ST content, but also to capture the information contained in the spectra related to other properties that can contribute to make each class different.

3.4 Detection of astringent and deastringed fruits

As in the prediction of ST content, the calyx, middle and apex areas were tested to distinguish A and DA fruits using PLS-DA models. The results of the classification models using hyperspectral imaging are presented in Table 5.

The calibration of the calyx and apex area models was performed using 18 LVs, while for the middle area model only 13 LVs were necessary. Furthermore, the internal CV of the middle area model presented the highest precision (86.6 %), then the apex area (82.6 %) and the calyx area model presented the lowest results, 78.1 %. This fact agrees with the previous results of the quantification of ST content, where the calyx area was the least precise part for this purpose.

The middle and calyx area models correctly classified more A fruits, 89.7 % and 78.5 % than DA fruits, 83.0 % and 77.7 %, respectively. In the case of the apex area, more DA fruits were correctly classified: 83.0 % versus 82.2 %.

The mean spectrum of each fruit of the test set was classified using the previously calibrated models. As in the calibration and CV, the model using the calyx area presented less precision, correctly classifying 83.3 % of A fruits and 77.8 % of DA fruits, and showing a total accuracy of 80.8 %. In the case of the middle and apex areas, their prediction showed similar results with 87.0 % of A fruits and 91.1 % and 88.9 % DA fruits being classified correctly. Therefore, the total accuracy of the middle and apex area models, 88.9 % and 87.9 %, was higher than that of the calyx area. This fact agrees with the results obtained in the quantification of ST, where the calyx area was the least accurate area for this purpose (Table 4).

Table 5. Results of the classifications using the calyx, middle and apex areas and all wavelengths

Area	#LV	Class	Calibration				Cross Validation				Prediction			
			#A	#DA	CC (%)	Acc (%)	#A	#DA	CC (%)	Acc (%)	#A	#DA	CC (%)	Acc (%)
Calyx	18	A	95	12	88.8	89.1	84	23	78.5	78.1	45	9	83.3	80.8
		DA	10	84	89.4		21	73	77.7		10	35	77.8	
Middle	13	A	101	7	94.4	91.5	96	11	89.7	86.6	47	7	87.0	88.9
		DA	11	83	88.3		16	78	83.0		4	41	91.1	
Apex	18	A	100	6	93.5	91.0	88	19	82.2	82.6	47	7	87.0	87.9
		DA	11	83	88.3		16	78	83.0		5	40	88.9	

#LV = number of latent variables; #A = number of astringent fruits; #DA = number of deastringed fruits; CC = correct classification; Acc = accuracy

Previous studies have been conducted to classify the fruits according to their astringency using spectral information. It is noteworthy that the best results in terms of ST prediction have been reported when values of ST content are high (Zhang et al., 2013; Altieri et al., 2017; Cortés et al., 2017, Munera et al., 2017). In this line, Noypitak et al. (2015) reported on a model in which a classification accuracy of 97.1% was achieved, assuming that the persimmon with an ST content lower than 0.8% is non-astringent. However, as mentioned in the introduction section, the threshold of ST to detect astringency is not established and is highly dependent not

394 only on the cultivar but also on the consumer's country of origin (Antoniolli et al., 2000;
395 Antoniolli et al., 2002; Yamada et al., 2002; Tessmer et al 2016). In 'Rojo Brillante' persimmon
396 it has been widely reported that sensorial astringency loss occurs when tannin content is lower
397 than 0.04% (Salvador et al 2007; Tessmer et al 2016). This means that the predictive models
398 previously reported would not be valid for this cultivar. In the present study the threshold
399 applied was 0.04% to guarantee the complete non-astringency of the fruits. Although the result
400 of the ST predictive model might seem a priori unsatisfactory (42.2 % of DA fruits correctly
401 classified), this is the first work in which such a low ST threshold has been established to
402 guarantee the non-astringency of the fruits. The results reveal that the higher the established ST
403 threshold is, the better the results provided by the predictive models are. This fact leads us to
404 think that other attributes, besides the ST content, may influence the spectral response of
405 persimmon.
406 Salvador et al. (2007) evaluated the physiological and structural changes that occur after
407 the deastringency treatment with high CO_2 concentrations in persimmon 'Rojo Brillante'
408 at different maturity stages. Some of the reported changes may affect the spectral information.
409 this way, a decline in the TSS, measured as ºBrix, occurs after deastringency treatment
410 concomitant to the drop in ST as a response to the deastringency process. On the other hand,
411 after the CO_2 treatment a significant increase in pH is observed. This rise in the pH value is
412 also related to the process by which soluble tannins, the acid components, become insoluble
413 the application of the treatment. It is noteorthy that the measurements of soluble solids in
414 persimmon are related to ST, but also to sugars and acids, are located between 720 nm and 820
415 nm, phenolic compounds are between 940 nm and 1000 nm, and the tannic acid peaks at 996
416 nm.
417 In addition, it must be taken into account that the cellular microstructure can have an
418 important effect on the spectral response. Hence, it has been reported that the deastringency
419 process causes important changes in the cell microstructure. The insolubilisation of tannins
420 occurs inside the vacuoles of tannin cells, which appeared to be filled with an insoluble material
421 (like a compact mass) (Salvador et al., 2007). Thus, depending on the level of insolubilisation

during the deastringency treatment, the number of cells in the parenchyma containing insoluble material will be greater or lower. Moreover, the CO_2 applied, in addition to triggering the insolubilisation of tannins, also brings about a progressive degradation of the structure, affecting the cell walls and integrity of the cell membranes. The adhesion bonds between some cells are lost in certain areas and the intercellular spaces are filled with a soluble material. This effect becomes greater as the treatment time increases (Salvador et al 2007; Novillo et al., 2014). It should be noted that the declining firmness that occurs during the maturity process of persimmon fruit has been associated with a gradual loss of parenchyma structure due to degradation of the cell wall and membrane (Salvador et al., 2007; Tessmer et al., 2016). In the same way, the effect of high concentrations of CO_2 on the cellular structure is related to a loss of firmness.

These structural changes associated with both the maturity stage and the CO_2 treatment may have an important effect on the spectra, since firmness is related to the water content (with absorption peaks at 750 nm and 970 nm) and the structural status of the cells parenchyma. This may have an influence on the way the light interacts with the cells and is transmitted through the fruit and hence the spectral response received by the spectrometer, which allowed A fruits to be separated from DA fruits.

Regarding the colour, the treatment with CO_2 did not cause any great changes in fruit skin for the earlier stages of fruit maturity, although small differences were observed in the last stage due to changes in carotenoids, anthocyanins and chlorophylls related to wavelengths 450–720 nm, 460 nm, 550–600 nm and 650–710 nm (Rajkumar et al., 2012). However, since the colour has not previously been evaluated to detect the astringency of the 'Rojo Brillante' persimmon, a PLS-DA model was calibrated using the HunterLab colour coordinates *L*, *a*, *b*. As a result, 66.7 % of A and 33.6 % of DA fruits were correctly classified, showing a total precision of 52.5 % (Table 6). This result indicates that traditional colour measures are not useful for the discrimination of A and DA fruits. However, from the results obtained using hyperspectral images, it is possible to present an alternative to those methods that are destructive, need chemical analysis, are subjective and only allow the inspection of a few samples per batch.

Table 6. Results of the classification of A and DA fruits using the colour information.

#LV	Class	Calibration				Cross Validation				Prediction			
		#A	#DA	CC (%)	Acc (%)	#A	#DA	CC (%)	Acc (%)	#A	#DA	CC (%)	Acc (%)
2	A	78	29	72.9	57.2	77	30	72.0	58.7	36	18	66.7	52.5
	DA	57	37	39.4		53	41	43.6		29	16	35.6	

#LV = number of latent variables; #A = number of astringent fruits; #DA = number of deastringed fruits; CC = correct classification; Acc = accuracy

3.4.1 Selection of optimal wavelengths

In order to reduce the complexity of the system, the number of wavelengths used should be reduced because a large number of wavelengths increases the acquisition time while it reduces the performance of classifiers (Friedman, 1994). Numerous techniques have been employed to deal with this issue, such as restricting the information to just a few bands which reveal the most variability and therefore the most significant information in the hyperspectral image (Du and Sun, 2006). In this study, the vector of the regression coefficients was used. A total of 23 optimal wavelengths were selected in the vector of each area, all of them being located across the VIS and NIR region (Figure 5).

The high number of wavelengths selected indicated that there are no specific ones that can be specifically linked to the tannins or other particular constituents related to astringency. Hyperspectral images show a high degree of collinearity and redundant information and this selection is probably a reduction of this information. More than half of the selected wavelengths for the three areas are located in the VIS region, which is related to the carotenoids, anthocyanins, chlorophylls and other pigments responsible for fruit colour, as previously commented. Several wavelengths were selected near the water absorption peaks, around 750 nm (first overtone of OH) and 970 nm (third overtone of OH) (Siedliska et al., 2018; Nicolaï et al., 2007; Williams and Norris, 1987). Other selected wavelengths are located around 850 nm, which is assigned to the absorption of acids and sugars (Yang et al., 2015). As commented earlier, phenolic compounds are located between 940–1000 nm and the absorption peak of

475 tannic acid is seen at 996 nm (Noypitak et al., 2015). Several selected wavelengths are located
476 in this region but it is not clear whether this corresponded to the ST content or to the water
477 absorption peak.

478 The optimised classification models were built using the selected wavelengths as input.
479 Results of the calibration are presented in Table 7. The models for the calyx and apex areas
480 were performed using 15 and 13 LVs, while only eight LVs were necessary to build the model
481 for the middle area. In this case, the increased accuracy in CV made the results more similar in
482 the calibration of the models. As in the case of the models built using the full spectra, the
483 internal CV of the middle area presented the highest accuracy (88.1%), then the apex area with
484 83.1% and the calyx area model presented the lowest results with only 78.6% of total accuracy.
485 In all cases, A fruits were detected better than DA fruits, which is in line with the principal aim
486 of detecting astringent fruits among those that have been submitted to a CO_2 treatment.

487 As in the classification performed using all wavelengths, the class of each fruit in the test set
488 was predicted by introducing the mean spectrum of the fruit into the previously optimised
489 models. In the case of the middle and apex areas, their prediction of A fruits showed similar
490 results between areas and using all and the optimal wavelengths, resulting in a correct
491 classification of 87.0% of A fruits. However, precision was lower for both areas in DA fruits,
492 with respect to the previous models, i.e. 86.7 %and 84.4% of DA fruits. Therefore, the total
493 accuracy of the middle and apex area models was 86.9% and 85.9%. Despite the reduction in
494 precision in the classification of DA fruits using fewer wavelengths, this is more desirable than
495 the contrary. If a DA fruit is classified as A, it can be treated again with CO_2, but if an A fruit is
496 classified as DA, this fruit goes directly to the consumer. In the case of the calyx area model,
497 81.5% of A and 82.2% of DA fruits were classified correctly. The total accuracy was a little
498 higher than when using all the wavelengths (81.8%), although it was again the least accurate of
499 the three areas.

500

501 Table 7. Results of the classification using the calyx, middle and apex areas and optimal
502 wavelengths selected

Area	#V	#LV	Class	Calibration				Cross Validation				Prediction			
				#A	#DA	CC (%)	Acc (%)	#A	DA	CC (%)	A (%)	#A	#DA	CC (%)	Acc (%)
Calyx	23	15	A	90	17	84.1	82.6	89	18	83.1	78.6	44	10	81.5	81.8
			DA	18	76	80.9		25	69	73.4		8	37	82.2	
Middle	23	8	A	97	10	90.7	90.0	96	11	89.7	88.1	47	7	87.0	86.9
			DA	10	84	89.4		13	81	86.2		6	39	86.7	
Apex	23	13	A	94	13	87.9	86.6	91	16	85.0	83.1	47	7	87.0	85.9
			DA	14	80	85.1		18	76	80.9		7	38	84.4	

#LV = number of latent variables; #A = number of astringent fruits; #DA = number of deastringed fruits; CC = correct classification; Acc = accuracy

4. CONCLUSIONS

The capability of VIS-NIR hyperspectral imaging to discriminate A and DA hard 'Rojo Brillante' persimmon fruits was investigated. Furthermore, as ST are heterogeneously distributed in the flesh of persimmon fruit, an individual study of three different areas of the fruit was carried out in order to find the most suitable to maximise the accuracy of the models.

The prediction of ST content in the fruits was performed using PLS-R models. The results obtained indicated that the model using the spectra of the apex area was the most accurate, R^2 of 0.71 with an RMSE of 0.18 and RPD 1.9. However, only 77.8% of A fruits and 42.2% of DA fruits were correctly classified **using PLS-R** when the threshold of 0.04% was applied **which was clearly insufficient**. Therefore, PLS-DA models were performed in order to maximise the separation between A and DA classes, which led to an improvement in the results. The most accurate models were those performed using middle and apex area spectra (88.9% and 87.9%), with a correct classification of 87.0% of A fruits and 91.1% and 88.9% of DA fruits, respectively. When the discrimination of the fruit was performed using colour information, the accuracy in the classification was only 66.7% for A and 33.6% for DA fruits.

To reduce the huge amount of data captured by the hyperspectral systems, the vector of the regression coefficients of the PLS-DA model of each area was used to identify the optimal wavelengths. As when using all wavelengths, the most accurate models were those involving

524 the middle and apex areas and 23 optimal wavelengths (86.9% and 85.9%), also with a correct
525 classification of 87.0% of A fruits and 86.7% and 84.4% of DA fruits, respectively.
526 According to these results, hyperspectral imaging combined with multivariate analysis has a
527 great potential as a tool for rapid and non-destructive control of effectiveness of the astringency
528 removal treatment applied to persimmon cv. 'Rojo Brillante'. Nevertheless, the results of this
529 study need further experimentation on a larger set of fruits grown in different areas and
530 harvested at different stages of ripeness before this could be effectively implemented in an in-
531 line system.
532
533 **Acknowledgements**
534 This work was partially funded by INIA and FEDER funds through project RTA2015-
535 00078-00-00. Sandra Munera thanks INIA for the FPI-INIA grant num. 43 (CPR2014-0082),
536 partially supported by European Union FSE funds.
537
538 **REFERENCES**
539 Altieri, G., Genovese, F., Tauriello, A. & Di Renzo, G.C. (2017). Models to improve the non-
540 destructive analysis of persimmon fruit properties by VIS/NIR spectrometry. *Journal of the*
541 *Science of Food and Agriculture 97,* 5302-5310.
542 Antoniolli, L.R., Castro, P.R.C., Kluge, R.A. & Scarpare Filho, J.A. (2000). Remoção da
543 adstringência de frutos de caqui 'Giombo' sob diferentes períodos de exposição ao vapor de
544 álcool etílico. *Pesquisa Agropecuária Brasileira, 35,* 2083-2091.
545 Antoniolli, L.R., Castro, P.R.C., Kluge, R.A. & Scarpare Filho, J.A. (2002). A remoção da
546 adstringência de frutos de caquizeiro 'Giombo' sob diferentes temperaturas. *Pesquisa*
547 *Agropecuária Brasileira, 37,* 687-691.
548 Arnal, L. & Del Río, M.A. (2004). Effect of cold storage and removal astringency on quality
549 of persimmon fruit (*Diospyros kaki*, L.) cv. Rojo brillante. *Food Science and Technology*
550 *International 10*, 179-185

551 Arnal, L. & Del Río, M.A. (2003). Removing astringency by carbon dioxide and nitrogen-
552 enriched atmospheres in persimmon fruit cv. 'Rojo brillante'. *Journal of Food Science 68*,
553 1516-1518.
554 Besada, C., Salvador, A., Arnal, L. & Martínez-Jávega, J.M. (2010). Optimization of the
555 duration of deastringency treatment depending on persimmon maturity. *Acta Horticulturae*
556 *858*, 69-74.
557 Besada, C., Arnal, L. & Salvador, A. (2008). Improving storability of persimmon cv. Rojo
558 Brillante by combined use of preharvest and postharvest treatments. Postharvest Biology
559 and Technology 50, 169-175
560 Cortés, V., Rodríguez, A. Blasco, J., Rey, B., Besada, C., Cubero, S., Salvador, A., Talens, P. &
561 Aleixos, N. (2017). Prediction of the level of astringency in persimmon using visible and
562 near-infrared spectroscopy. *Journal of Food Engineering 204*, 27-37.
563 Du, C.J. & Sun, D.W. (2006). Learning techniques used in computer vision for food quality
564 evaluation: a review. *Journal of Food Engineering, 72*, 39–55.
565 Erkinbaev, C., Henderson, K., & Paliwal, J. (2017). Discrimination of gluten-free oats from
566 contaminants using near infrared hyperspectral imaging technique. *Food Control 80*, 197-
567 203.
568 FAOSTAT (2016). http://www.fao.org/faostat/en/#data/QC - Accessed 02.11.18
569 Folch-Fortuny, A., Prats-Montalbán, J.M., Cubero, S., Blasco, J. & Ferrer, A. (2016). VIS/NIR
570 hyperspectral imaging and N-way PLS-DA models for detection of decay lesions in citrus
571 fruits. *Chemometrics and Intelligent Laboratory Systems 156*, 241-248.
572 Friedman J.H. (1994) An Overview of Predictive Learning and Function Approximation. In:
573 From Statistics to Neural Networks. Cherkassky V., Friedman J.H., Wechsler H. (eds)
574 NATO ASI Series, 136. Springer, Berlin, Heidelberg.
575 Gat, N. (2000). Imaging spectroscopy using tunable filters: A review. Technical report, Opto-
576 Knowledge Systems Inc. OKSI.

577 Geladi, P. L. M. (2007). Calibration standards and image calibration. In H. F. Grahn & P.
578 Geladi (Eds.), Techniques and applications of hyperspectral image analysis (pp. 203–220).
579 Chichester: Wiley.
580 Gómez-Sanchis J, Lorente D, Soria-Olivas E, Aleixos N, Cubero S, Blasco J (2014)
581 Development of a hyperspectral computer vision system based on two liquid crystal
582 tuneable filters for fruit inspection. Application to detect citrus fruits decay. *Food and*
583 *Bioprocess Technology, 7*, 1047-1056.
584 Gorini, F. L. & Testoni, A. (1988). Maturazione, raccolta, conservazione e trasformazione
585 dei frutti di kaki. *Agricoltura e Ricerca 95*, 81–88.
586 López-Maestresalas, A., Keresztes, J.C., Goodarzi, M., Arazuri, S. & Saeys, W. (2016). Non-
587 destructive detection of blackspot in potatoes by Vis-NIR and SWIR hyperspectral imaging.
588 *Food Control 70*, 229-241.
589 Lorente, D., Aleixos, N., Gómez-Sanchis, J., Cubero, S., García-Navarrete, O. L. & Blasco, J.
590 (2012). Recent advances and applications of hyperspectral imaging for fruit and vegetable
591 quality assessment. *Food Bioprocess Technology 5*, 1121–1142.
592 Lu, R. & Peng, Y. (2006). Hyperspectral scattering for assessing peach fruit firmness.
593 *Biosystems Engineering 93*, 161-171.
594 Malegori, C., Nascimento, E. J., Tonetto de Freitas, S., Pimentel, M. F., & Casiraghi, E. (2017).
595 Comparing the analytical performances of Micro-NIR and FT-NIR spectrometers in the
596 evaluation of acerola fruit quality, using PLS and SVM regression algorithms. *Talanta 165*,
597 112-116.
598 Matsuo, T. & Itoo, S. (1982). A model experiment for de-astringency of persimmon fruit with
599 high carbon dioxide treatment: In vitro gelation of kaki-tannin by reacting with
600 acetaldehyde. *Agricultural and Biological Chemistry 46*, 683-689
601 Mehmood, T., Liland, K. H., Snipen, L. & Sæbø, S. (2012). A review of variable selection
602 methods in Partial Least Squares Regression. *Chemometrics and Intelligent Laboratory*
603 *Systems 118*, 62–69.

Mobaraki, N. & Amigo, J.M. (2018). HYPER-Tools. A graphical user-friendly interface for hyperspectral image analysis. *Chemometrics and Intelligent Laboratory Systems 172*, 174-187.

Munera, S., Amigo, J.M., Aleixos, N., Talens, P., Cubero, S. & Blasco, J. (2018). Potential of VIS-NIR hyperspectral imaging and chemometric methods to identify similar cultivars of nectarine. *Food Control 86*, 1-10.

Munera, S., Besada, C., Aleixos, N., Talens, P., Salvador, A., Da-Wen, S., Cubero, S. & Blasco, J (2017). Non-destructive assessment of the internal quality of intact persimmon using colour and VIS/NIR hyperspectral imaging. *LWT - Food Science and Technology 77*, 241-248.

Nicolaï, B. M., Beullens, K., Bobelyn, E., Peirs, A., Saeys,W., Theron, K. I., et al. (2007). Nondestructive measurement of fruit and vegetable quality by means of NIR spectroscopy: A review. *Postharvest Biology and Technology 46*, 99-118.

Novillo, P., Salvador, A., LLorca, E., Hernando, I. & Besada, C. (2014). Effect of CO_2 deastringency treatment on flesh disorders induced by mechanical damage in persimmon. Biochemical and microstuctural studies. *Food Chemistry*, *145*, 454-463.

Noypitak, S., Terdwongworakul, A., Krisanapook, K. & Kasemsumran, S. (2015). Evaluation of astringency and tannin content in 'Xichu' persimmons using near infrared spectroscopy. *International Journal of Food Properties 18*, 1014–1028.

Rajkumar, P., Wang, N., EImasry, G., Raghavan, G.S.V. & Gariepy, Y. (2012). Studies on banana fruit quality and maturity stages using hyperspectral imaging. *Journal of Food Engineering 108*, 194–200.

Rinnan, Å., van den Berg, F. & Engelsen, S. B. (2009). Review of the most common pre-processing techniques for near-infrared spectra. *Trends in Analytical Chemistry 28*, 1201-1222.

Siedliska, A., Baranowski, P., Zubik, M., Mazurek, W. & Sosnowska, B. (2018). Detection of fungal infections in strawberry fruit by VNIR/SWIR hyperspectral imaging. *Postharvest Biology and Technology 139*, 115-126.

632 Salvador, A., Arnal, L., Besada, C., Larrea, V., Quiles, A. & Pérez-Munuera, I. (2007).
633 Physiological and structural changes during ripening and deastringency treatment of
634 persimmon cv. 'Rojo Brillante'. *Postharvest Biology and Technology 46*, 181–188.
635 Salvador, A., Arnal, L., Besada, C., Larrea, V., Quiles, A. & Pérez-Munuera, I. (2008). Reduced
636 effectiveness of the treatment for removing astringency in persimmon fruit when stored at
637 15 ºC. Physiological microstructural study. *Postharvest Biology and Technology 49*, 340–
638 347.
639 Taira, S., Ono, M. & Matsumoto, N. (1997). Reduction of persimmon astringency by complex
640 formation between pectin and tannins. *Postharvest Biology and Technology 12*, 265-271.
641 Taira, S. (1995). Astringency in persimmon. In: Linskens, H.F., Jackson, J.F. (Eds.), Fruit
642 analysis (pp 97–110). Hannover, Germany: Springer.
643 Tessmer, M.A., Besada, C., Hernando, I., Appezzato-da-Glória, B., Quiles, A. & Salvador, A.
644 (2016). Microstructural changes while persimmon fruits mature and ripen. Comparison
645 between astringent and non-astringent cultivars. *Postharvest Biology and Technology 120*,
646 52-60.
647 Vinzi, V., Chin, W. W., Henseler, J. & Wang, H. (2010). Handbook of partial least squares.
648 Wang, H. (Ed.). Berlin: Springer.
649 Williams, P., & Norris, K. (1987). Near-infrared Technology in the Agricultural and Food
650 Industries. St. Paul, USA: American Association of Cereal Chemists.
651 Williams, P.C. (1987). Variables affecting near-infrared reflectance spectroscopic analysis. In:
652 Williams, P., Norris, K. (Eds.), Near-infrared Technology in the Agricultural and Food
653 Industries. American Association of Cereal Chemists, St. Paul, MN, pp. 143e166.
654 Xiaobo, Z., Jiewen, Z., Povey, M.J.W., Holmes, M. & Hanpin, M. (2010). Variables selection
655 methods in near-infrared spectroscopy. *Analytica Chimica Acta 667*, 14-32.
656 Yamada, M., Taira, S., Ohtsuki, M., Sato, A., Iwanami, H., Yakushiji, H., Wang, R., Yang, Y.
657 & Li, G. (2002). Varietal differences in the ease of astringency removal by carbon dioxide
658 gas and ethanol vapor treatments among Oriental astringent persimmons of Japanese and
659 Chinese origin. *Scientia Horticulturae, 94*, 63-72.

Yang, C. H., Sun, D. W., Pu, H., Wang, N. N. & Zhu, Z. (2015). Rapid detection of anthocyanin content in lychee pericarp during storage using hyperspectral imaging coupled with model fusion. *Postharvest Biology and Technology 103*, 55-65.

Zhang, P., Xue, Y., Li, J., Feng, X. & Wang, B. (2013). Research on non-destructive measurement of firmness and soluble tannin content of 'mopanshi' persimmon using Vis/NIR diffuse reflection spectroscopy. *Acta Horticulturae 996*, 447-452.

FIGURES

Figure 1. Hyperspectral images of the three areas of persimmon fruit acquired at 710 nm.

Figure 2. Example of external and internal appearance of the fruit before and after de-astringency treatment. Visualisation of the distribution of ST using the alternative method of foils soaked in $FeCl_3$. *A = astringent; DA = deastringed*

Figure 3. Mean pre-treated spectra of each area of astringent (A) and deastringed (DA) fruits.

Figure 4. Prediction of the soluble tannins content in test set fruit using the apex area.
The red lines indicate the threshold value of 0.04%

Figure 5. Regression coefficients vector of the PLS-DA model of each area with the optimal wavelengths selected.

Figure
Click here to download high resolution image

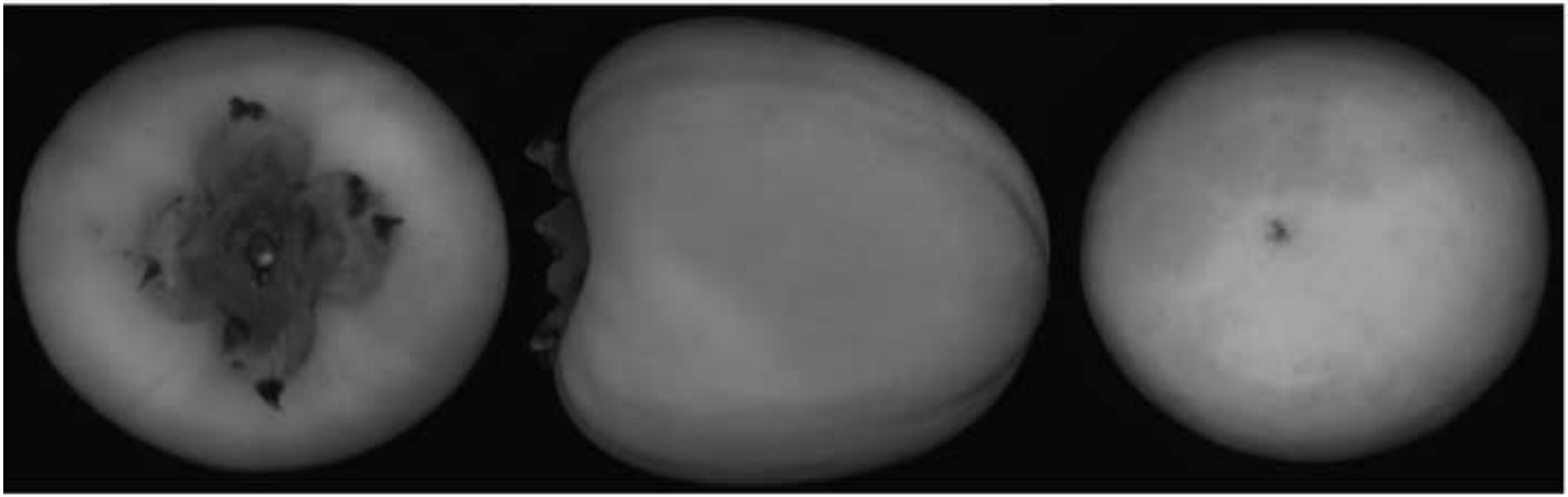

Figure

Click here to download high resolution image

Figure

Click here to download high resolution image

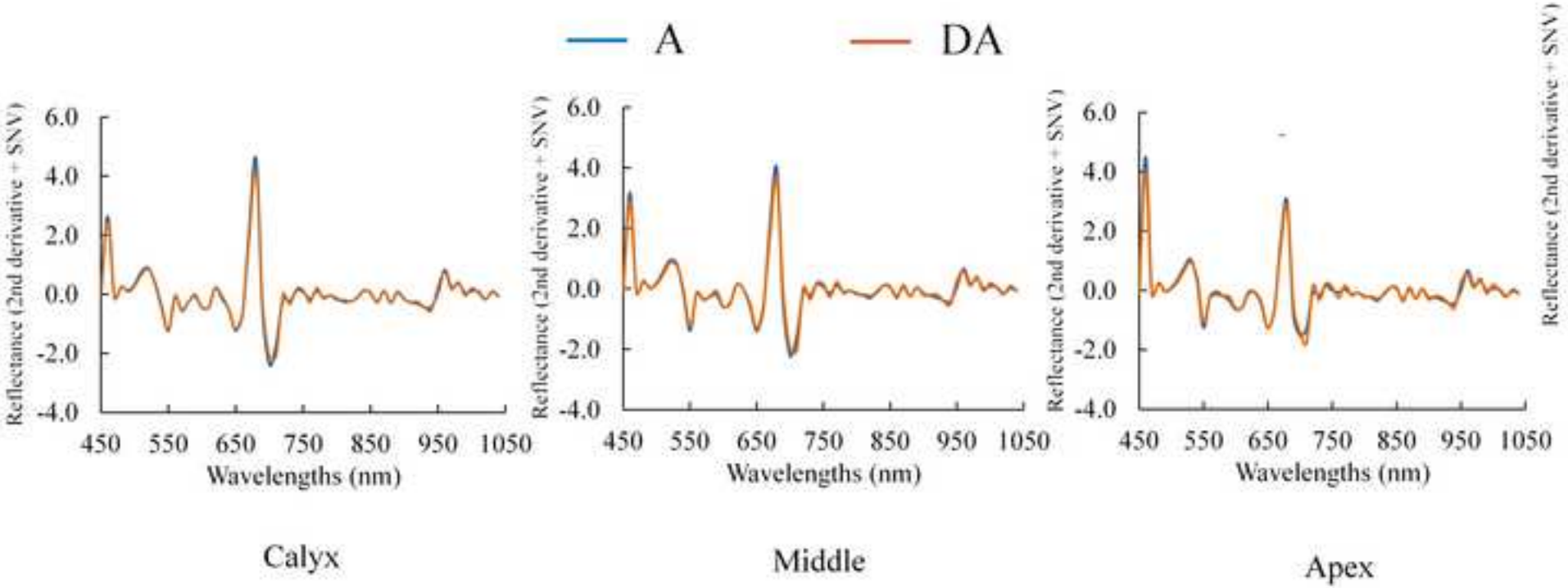

Figure

Click here to download high resolution image

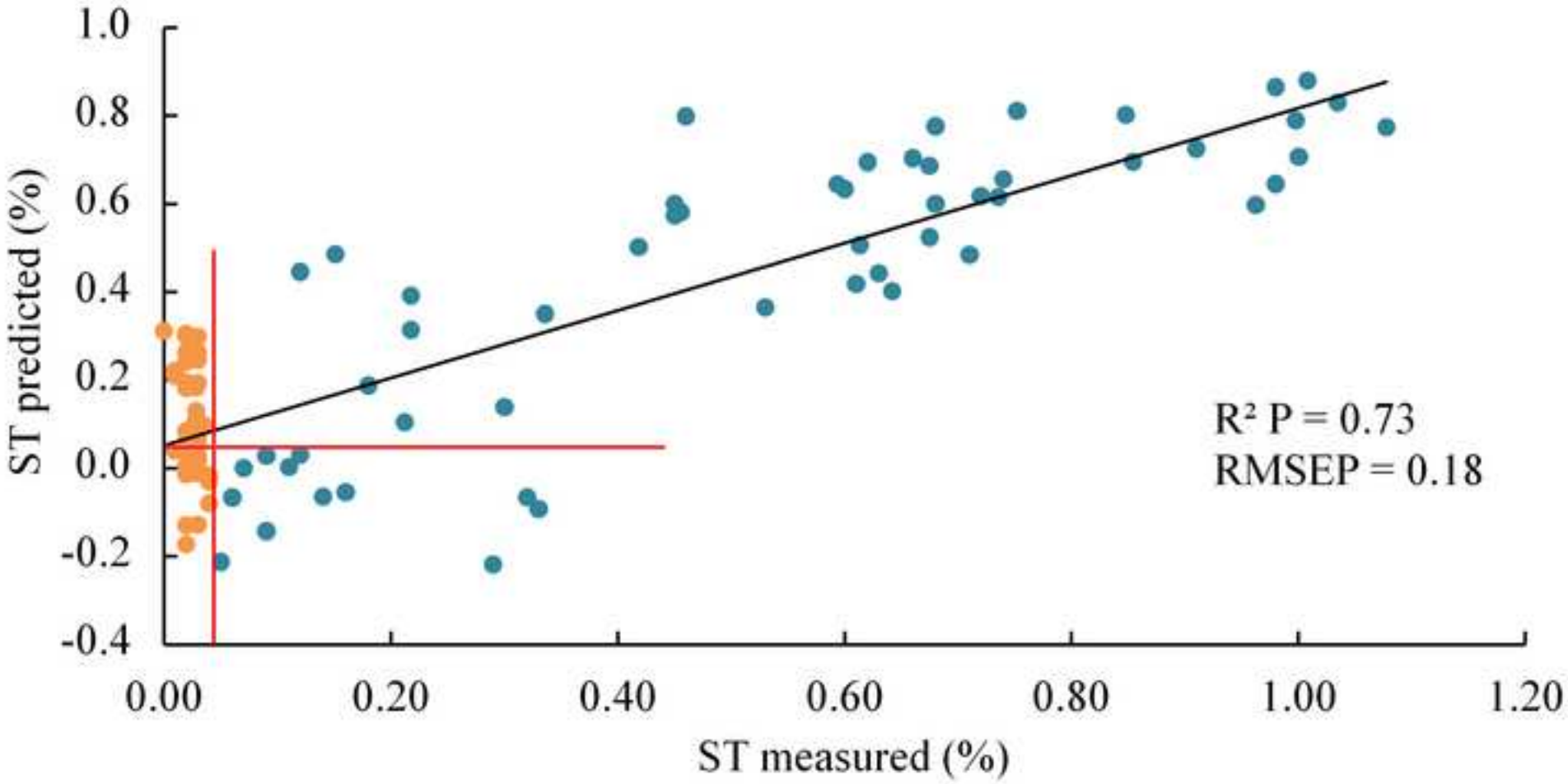

Figure

Click here to download high resolution image